energies

MDPI

Article

Determination of Film Cooling Effectiveness and Heat Transfer Coefficient Simultaneously on a Flat Plate

Mingjie Zhang

State Key Laboratory for Turbulence and Complex Systems, College of Engineering, Peking University, Beijing 100871, China; mezhang@pku.edu.cn

Abstract: In this paper, flat plate film cooling with two rows of compound angle cylindrical film cooling holes was investigated. A data processing method was evaluated which could determine the film cooling effectiveness and heat transfer coefficient simultaneously from the transient wall temperature data. The method was based on solving an inverse problem of the one-dimensional transient heat conduction equation. To evaluate the performance of the method, wall temperature data were obtained using the known film cooling effectiveness and heat transfer coefficient data as the convection boundary condition. Then, the method was applied to calculate the film cooling effectiveness and heat transfer coefficient based on the wall temperature data. Different blowing ratios, heat transfer coefficients, mainstream temperatures, and material thermal conductivities were investigated. In general, the data and calculation were in good agreement. It was found that the error decreased when the heat transfer coefficient increased and the material thermal conductivity decreased. The percentage error of the span-wise averaged film cooling effectiveness was mainly between 0% and 10%, and the percentage error of the span-wise averaged heat transfer coefficient was mainly between 0% and 4%.

Keywords: film cooling effectiveness; heat transfer coefficient; transient heat conduction

Citation: Zhang, M. Determination of Film Cooling Effectiveness and Heat Transfer Coefficient Simultaneously on a Flat Plate. *Energies* **2022**, *15*, 4144. https://doi.org/10.3390/en15114144

Academic Editors: Jiang Lei and Phillip Ligrani

Received: 16 May 2022
Accepted: 2 June 2022
Published: 4 June 2022

1. Introduction

Gas turbines are designed with very high turbine inlet temperatures to improve thermal efficiency and power output. Film cooling is a widely used cooling technology to protect turbine blades from hot gas under high temperature and pressure conditions. Reviews on film cooling research can be found in [1–4].

Film cooling effectiveness and heat transfer coefficient are two important variables used to evaluate film cooling performance. Some methods can determine the film cooling effectiveness and heat transfer coefficient simultaneously in a transient experiment. Vedula and Metzger [5] proposed a transient liquid crystal technique based on the analytical solution of the one-dimensional semi-infinite transient heat conduction equation. Ekkad et al. [6] developed a transient infrared thermography technique to determine the film cooling effectiveness and heat transfer coefficient simultaneously, using the measured wall temperature at two different times in a single test. A turbine blade leading edge model with a single film cooling hole was studied. Many data processing methods [7–9] can calculate the heat flux from the measured wall temperature. O'Dowd et al. [10] studied the heat transfer measurement technique for a transonic turbine blade tip. Heat flux was calculated from the measured wall temperature in the experiments, and the heat flux versus wall temperature curve was used to calculate the adiabatic wall temperature and heat transfer coefficient by linear fitting. Peck et al. [11] evaluated the errors of the linear fitting method in calculating the film cooling effectiveness and heat transfer coefficient and presented a method that could be used when the wall temperature was close to the adiabatic wall temperature in the experiments.

Flat plate film cooling with compound angle holes has been studied by many researchers. Schmidt et al. [12] and Sen et al. [13] measured the film cooling effectiveness

and heat transfer coefficient for a flat plate with one row of 60° compound angle film cooling holes, respectively. The coolant to mainstream momentum flux ratio varied from 0.16 to 3.9. The film cooling effectiveness was measured as the adiabatic effectiveness in steady-state experiments at DR = 1.6. The heat transfer coefficient was obtained by measuring the temperature on a constant heat flux surface at DR = 1.0. It was found that, at higher momentum flux ratios, the compound angle film cooling holes provided both higher film cooling effectiveness and heat transfer coefficients than the simple angle film cooling holes. Ekkad et al. [14,15] investigated flat plate film cooling with one row of cylindrical film cooling holes. Three compound angles of 0°, 45°, and 90° were tested. The blowing ratio M = 0.5, 1.0, and 2.0. The film cooling effectiveness and heat transfer coefficient were determined using a transient liquid crystal technique [16] through two separate transient experiments. The results showed that compound angle holes provided higher film cooling effectiveness than simple angle holes, and the heat transfer coefficient increased as the compound angle increased from 0° to 90°. Chen et al. [17] measured the film cooling effectiveness for a flat plate with one row of cylindrical or fan-shaped film cooling holes using the pressure-sensitive paint technique. The compound angle was 45°. The blowing ratio M varied from 0.3 to 2.0, and the density ratio DR = 1.0, 1.5, and 2.0. Film cooling effectiveness of the compound angle cylindrical holes was higher than that of the simple angle cylindrical holes. Laroche et al. [18] experimentally and numerically studied the flow field and heat transfer of a multiperforated plate with 90° compound angle holes. The results showed that the numerical simulations underestimated the mixing between the jets and freestream. Yao et al. [19–21] investigated the effects of spanwise distance, streamwise distance, density ratio, and mainstream incidence angle on the film cooling effectiveness of double-jet film cooling on a flat plate using the pressure-sensitive paint technique. The flow field and film cooling effectiveness were measured, and the interaction between the two jets was studied. It was found that the anti-kidney vortex effect could benefit the film cooling performance at proper incidence angles. Hang et al. [22] numerically studied a double-jet film cooling design on a turbine vane at different spanwise distances and incidence angles. The results showed that the design could restrain the jet detachment and improve the film coverage. Wang et al. [23] measured the film cooling effectiveness for a flat plate with two rows of 45° compound angle cylindrical film cooling holes using the pressure-sensitive paint technique. The density ratio DR = 1.0, 1.5, and 2.0, and the blowing ratio M = 0.5, 1.0, 1.5, and 2.0. Zhang et al. [24] presented an inverse method for simultaneously calculating the recovery temperature and heat transfer coefficient of aerodynamic heating. The method was to solve an inverse problem of the one-dimensional transient heat conduction equation with the convection boundary condition, using the measured wall temperature in a transient wind tunnel test. Aerodynamic heating on a flared cone at Mach 6 was considered. The infrared thermography technique was used to measure the wall temperature on the flared cone in the experiments.

In this study, flat plate film cooling with two rows of compound angle cylindrical film cooling holes, studied by Wang et al. [23], was considered. The novelty of this study was that it evaluated a heat transfer data processing method that was able to obtain the film cooling effectiveness and heat transfer coefficient simultaneously from the transient wall temperature data in an experiment. The advantage of this method is that it can be applied when the wall temperature data at several times is known, instead of the whole transient wall temperature history. In addition, the method can be carried out with time-dependent mainstream temperature and coolant temperature. The procedure of the method was presented in detail. The experimentally measured film cooling effectiveness and numerically calculated heat transfer coefficient data were used to generate the transient wall temperature data by solving the three-dimensional transient heat conduction equation. The method was then evaluated at different blowing ratios, heat transfer coefficients, mainstream temperatures, and material thermal conductivities.

2. Materials and Methods

In this section, the inverse method to simultaneously calculate the film cooling effectiveness and heat transfer coefficient presented by Zhang et al. [24] was introduced, based on solving the one-dimensional transient heat conduction equation, that can be written as

$$\frac{\partial T}{\partial t} = \frac{k}{\rho C_p}\frac{\partial^2 T}{\partial z^2} \tag{1}$$

where T is the temperature, t is the time, z is in the inward-pointing normal direction of the wall, k is the material thermal conductivity, ρ is the material density, and Cp is the material specific heat capacity. The convection boundary condition is used on the wall ($z = 0$), and the adiabatic wall boundary condition is used on the internal surface ($z = L$), where L is the wall thickness. Equation (1) is solved by the MATLAB one-dimensional parabolic and elliptic partial differential equations solver. The heat transfer coefficient and film cooling effectiveness can be written as

$$h = \frac{q}{T_{aw} - T_w} \tag{2}$$

$$\eta = \frac{T_{aw} - T_m}{T_c - T_m} \tag{3}$$

where h is the heat transfer coefficient, η is the film cooling effectiveness, q is the heat flux on the wall, T_w is the wall temperature, T_{aw} is the adiabatic wall temperature, T_m is the mainstream temperature, and T_c is the coolant temperature. When η, h, T_m, and T_c are known, the convection boundary condition on the wall can be applied.

The procedure of the method includes four steps. For an interval (t_a, t_b) that η and h are constants, the goal is to find a pair of η and h so that the calculated T_w using η and h as the convection boundary condition by solving Equation (1) approaches the known T_w in the time interval.

(1) A series of times t_i in (t_a, t_b) is selected and the initial value of η is guessed.
(2) For a guessed η and given t_i, the corresponding h_i can be calculated so that the reconstructed T_w based on η and h_i is equal to the measured T_w at time t_i. In the calculation process, the time interval is from t_a to t_i. To calculate h_i, the approach is to find and narrow down an interval ($h_{i,n}$, $h_{i,n+1}$) by iteration, so that T_w is between $T_{w,n}$ and $T_{w,n+1}$. Here, n is the iteration number, and $T_{w,n}$ and $T_{w,n+1}$ are the reconstructed wall temperatures at time t_i based on $h_{i,n}$ and $h_{i,n+1}$, respectively.
(3) A series of h_i can be obtained for the guessed η, and the slope of the h_i curve as a function of t_i can be calculated.
(4) A pair of η and h can be obtained when the slope of the h_i curve is close to zero. The approach is to narrow down an interval ($\eta_{,n}$, $\eta_{,n+1}$), so that at $\eta_{,n}$ and $\eta_{,n+1}$ the slopes are in opposite signs. Here, $\eta_{,n}$ and $\eta_{,n+1}$ are the guessed film cooling effectiveness, and n is the iteration number. When the slope is close to zero, the reconstructed wall temperature based on η and h will be close to the known wall temperature at times t_i, and in the interval (t_a, t_b).

The inverse method can be carried out with time-dependent mainstream temperature and coolant temperature, where the film cooling effectiveness and heat transfer coefficient are constants.

We considered the flat plate film cooling with two rows of compound angle cylindrical film cooling holes, as studied by Wang et al. [23]. The measured film cooling effectiveness data with density ratio $DR = 2.0$ and blowing ratio $M = 0.5$, 1.0, and 1.5 were used. To evaluate the performance of the method, the film cooling effectiveness and heat transfer coefficient data were given, and the transient wall temperature data were generated.

Figure 1 shows the flat plate geometry with two film cooling holes. For the flat plate design, the hole-to-hole spacing in the same row was 0.024 m; one film cooling hole for each row is shown. The mainstream was in the y-direction, and the mainstream velocity was 21 m/s. The coordinate origin was at the center of the film cooling hole in the second

row. The film cooling hole diameter d was 0.004 m, and the distance between the two holes in the y-direction was 0.012 m. The distance between the two side walls was 0.024 m, and the thickness of the flat plate was 0.01 m. The film cooling hole compound angle to the mainstream $\beta = 45°$, and the inclination angle to the top wall $\alpha = 30°$. More information on the flat plate design and flow conditions can be found in Wang et al. [23].

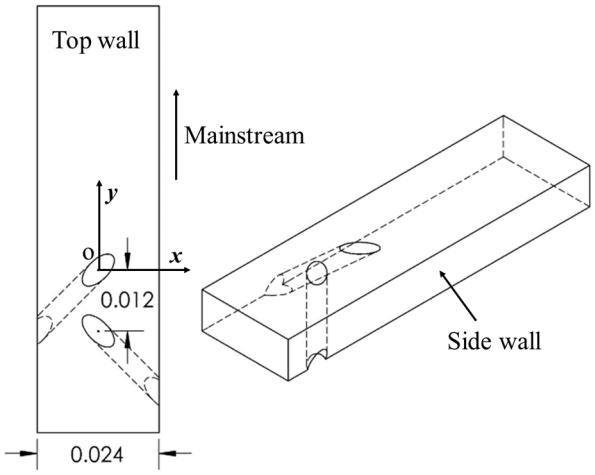

Figure 1. Flat plate geometry and coordinate.

Heat transfer coefficient data were obtained by CFD simulations, using the shear stress transport (SST) turbulent model. Wall temperature data were generated using the measured film cooling effectiveness and CFD calculated heat transfer coefficient data. We used the partial differential equation toolbox in MATLAB to solve the three-dimensional transient heat conduction equation. The solid domain is shown in Figure 1. The convection boundary condition with given η, h, T_m, and T_c was used on the top wall, and the adiabatic wall boundary condition was used on the other walls. The solid material density was 1300 kg/m^2, and the specific heat capacity was 1470 J/(kg·°C). The coolant temperature Tc was 300 K. The time interval was from t = 0 s to 20 s. The initial temperature field T_i at t = 0 s was 300 K. For transient experiments, the flow conditions such as h, T_m, and T_c can vary in the beginning period. In that case, the initial temperature field T_i needs to be calculated using the wall temperature in the beginning period as the temperature boundary condition.

To evaluate the performance of the method, ten cases with different values of blowing ratio M, mainstream temperature T_m, heat transfer coefficient h, and material thermal conductivity k were calculated, as presented in Table 1. Here, h_0 is the heat transfer coefficient by CFD simulations. For cases 1 to 9, common plastic material as used with k = 0.2 W/(m·K); for case 10, thermal insulation material was used with k = 0.05 W/(m·K). For cases 1, 2, and 3, the mainstream temperature was 320 K, the heat transfer coefficient was h_0, and the blowing ratio M varied from 0.5, 1.0, to 1.5. The experiments were carried out using a large-scale test section in a low-speed wind tunnel. In other experimental conditions, the scale of h can be different. For cases 4 and 5, the effect of h value was considered. For cases 6 and 7, the differences between the mainstream temperature and the coolant temperature were 10 K and 40 K, respectively. For case 8, T_m was a linear function of time; for case 9, T_m was a quadratic function of time, where T_m is 300 K at t = 0 s and 320 K at t = 20 s. In the calculation process, for cases 1–7 and case 10, the t_i series included eight points evenly distributed from 1 s to 20 s. For cases 8 and 9, the t_i series included eight points evenly distributed from 10 s to 20 s, as the difference between T_m and T_w was small (from 0 s to 10 s) for cases 8 and 9.

Table 1. Test cases.

Case	M	T_m (K)	h	k (W/mK)
1	0.5	320	h_0	0.2
2	1.0	320	h_0	0.2
3	1.5	320	h_0	0.2
4	1.0	320	$0.5\,h_0$	0.2
5	1.0	320	$2\,h_0$	0.2
6	1.0	310	h_0	0.2
7	1.0	340	h_0	0.2
8	1.0	$300 + t$	h_0	0.2
9	1.0	$300 + 2t - 0.05t^2$	h_0	0.2
10	1.0	320	h_0	0.05

3. Results

Temperature and heat flux fields at different y/d and t for case 2 are shown in Figure 2. The curves represent the temperature contours, and the red arrows represent the heat flux vectors in the x-z plane. For $y/d = 2$, at $-1 < x/d < 1$, large value of heat flux in the x-direction was observed. When y/d increased from 2 to 8, the lateral heat conduction and the heat flux in the x-direction decreased since the local variation of η and h decreased.

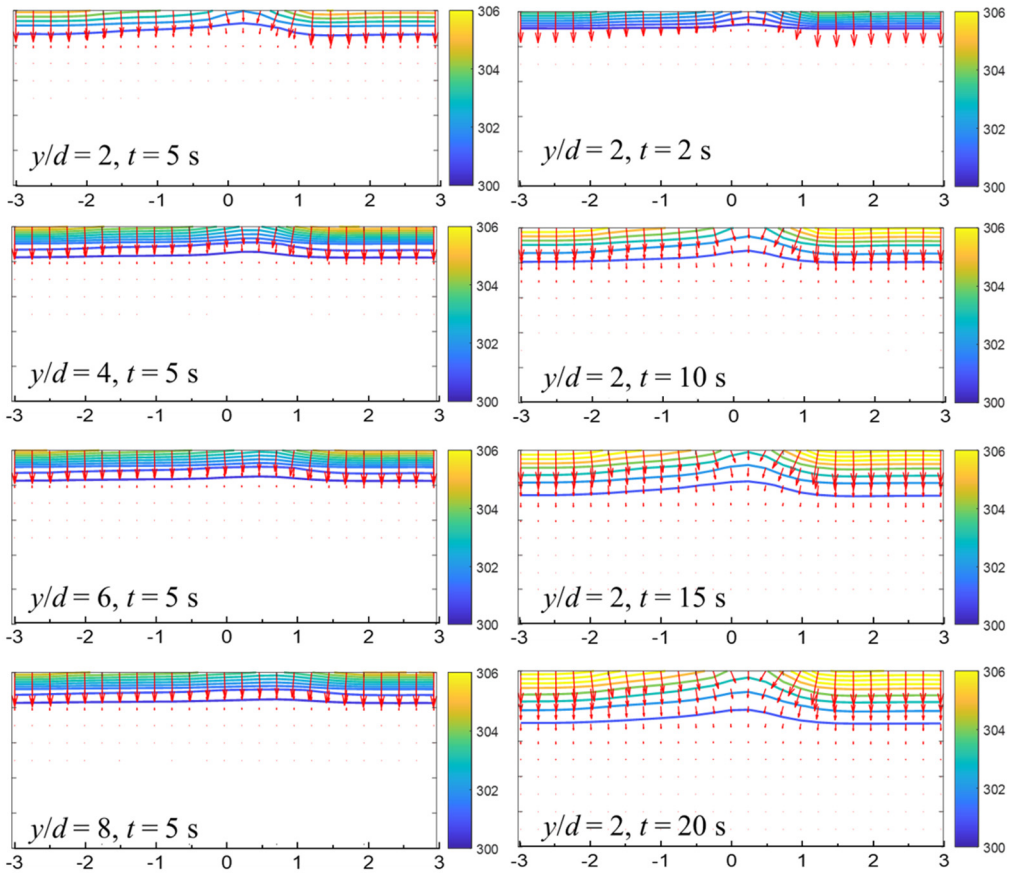

Figure 2. Temperature and heat flux fields at different y/d and t for case 2.

Figure 3 presents the comparison of the wall temperature time series between the data and calculation with different x/d at y/d = 4 for case 2. Here, the calculated wall temperature was reconstructed using the calculated film cooling effectiveness and heat transfer coefficient. A good agreement between the data and calculation was achieved. At x/d = 0 and 0.5, the wall temperature was low because of high film cooling effectiveness.

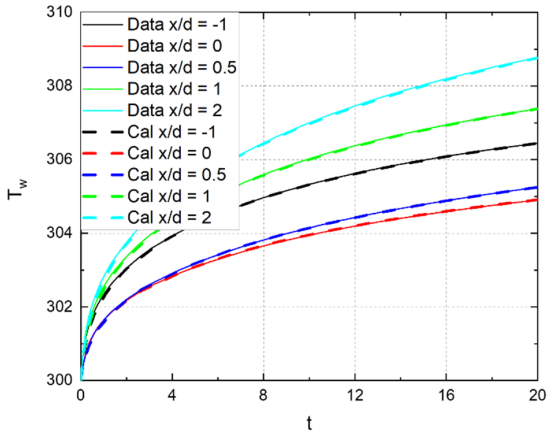

Figure 3. Comparison of wall temperature between the data and calculation with different *x/d* and *t* at *y/d* = 4 for case 2.

Comparisons of heat transfer coefficient and film cooling effectiveness contours between the data and calculation for cases 1, 2, and 3 at different blowing ratios are shown in Figures 4 and 5, respectively. Errors of calculated heat transfer coefficient and film cooling effectiveness contours at different blowing ratios are shown in Figure 6. In the figure, h and η are the known data, and h_{cal} and η_{cal} are the calculation. Overall, the contours were similar between the data and calculation. After each film cooling hole, two high heat transfer coefficient regions were observed, where the calculation was higher than the data. In the region between the two high heat transfer coefficient regions, the calculation was lower than the data.

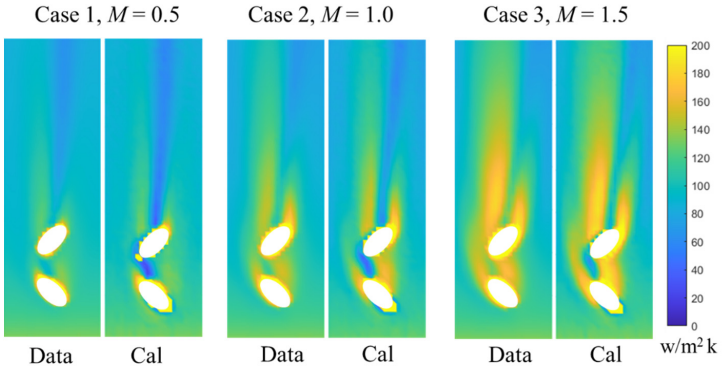

Figure 4. Comparison of heat transfer coefficient contours between the data and calculation at different *M*.

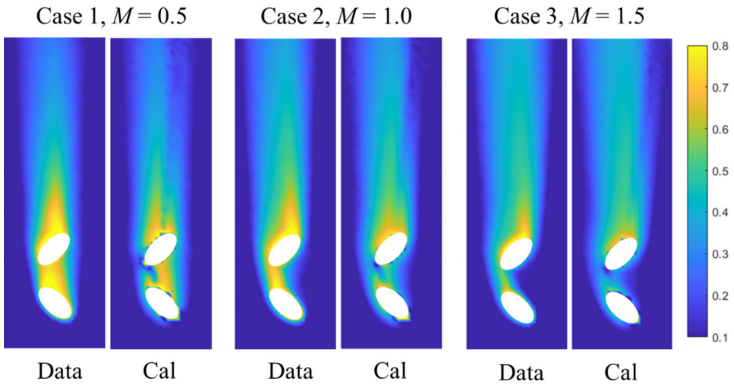

Figure 5. Comparison of film cooling effectiveness contours between the data and calculation at different *M*.

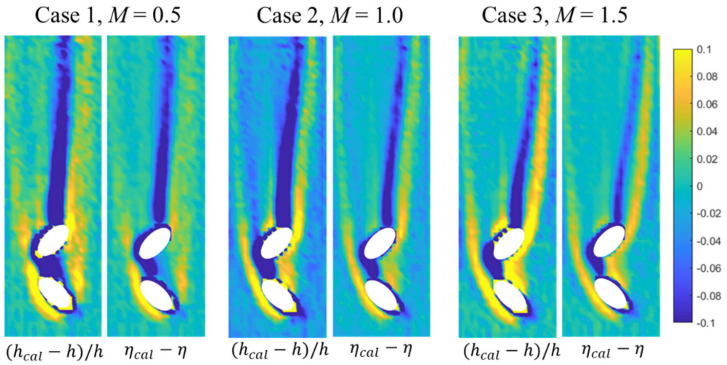

Figure 6. Errors of calculated heat transfer coefficient and film cooling effectiveness at different *M*.

The comparison of heat transfer coefficient and film cooling effectiveness between the data and calculation at different blowing ratios and *y/d* is shown in Figure 7. A large difference between the data and calculation was observed at $-0.5 < x/d < 1$, because of the lateral heat conduction in this region, as shown in Figure 2. The comparison of span-wise averaged heat transfer coefficient and film cooling effectiveness for cases 1, 2, and 3 at different blowing ratios is shown in Figure 8, where the data and calculation were in very good agreement.

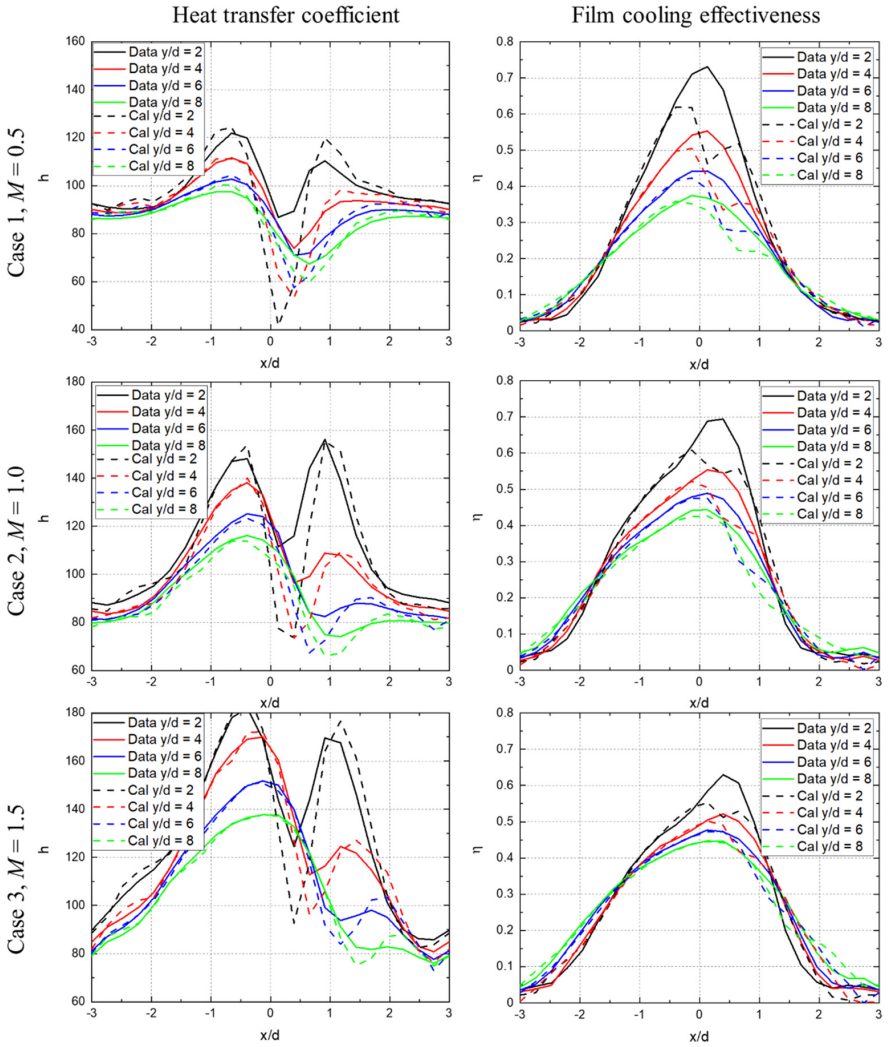

Figure 7. Comparison of heat transfer coefficient and film cooling effectiveness between the data and calculation at different *M* and *y/d*.

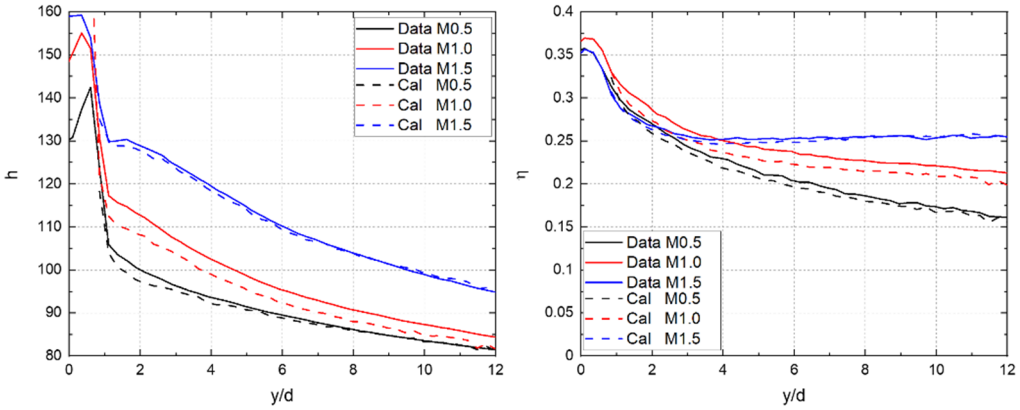

Figure 8. Comparison of span-wise averaged heat transfer coefficient and film cooling effectiveness between the data and calculation at different M for cases 1, 2, and 3.

Figures 9 and 10 present errors of calculated heat transfer coefficient and film cooling effectiveness contours at M = 1.0 for cases 4 to 10, respectively. For cases 4 and 5, errors decreased when h increased from 0.5 h_0 to 2 h_0. For cases 6 to 9, different mainstream temperatures ere tested. For case 10, local errors decreased significantly when k decreased from 0.2 W/(m·K) to 0.05 W/(m·K). At k = 0.05 W/(m·K), the local percentage error of h and the local error of η were mainly less than 6% and 0.04, respectively.

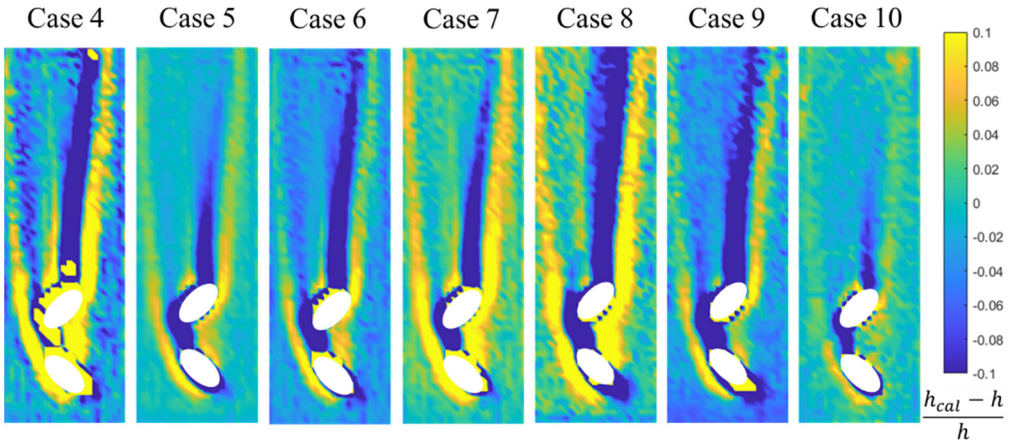

Figure 9. Errors of calculated heat transfer coefficient at M = 1.0.

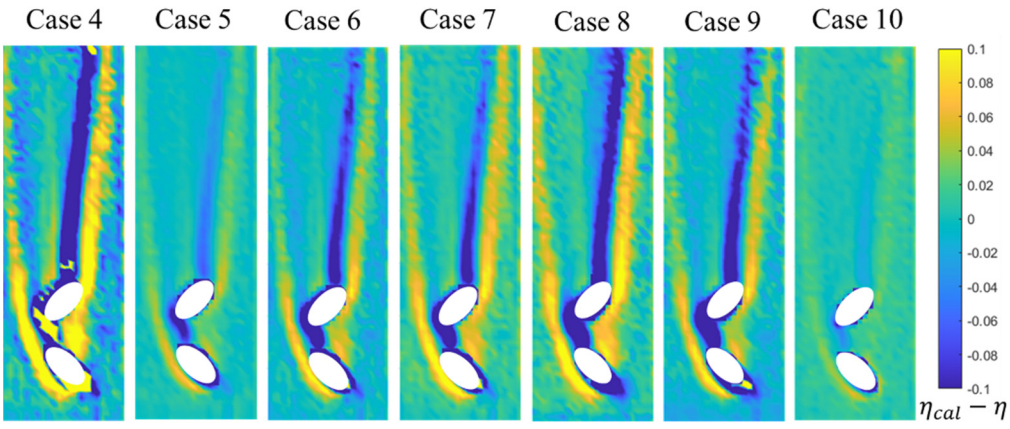

Figure 10. Errors of calculated film cooling effectiveness at M = 1.0.

Figure 11 shows errors of span-wise averaged heat transfer coefficient and film cooling effectiveness. In general, the calculations agreed well with the data. For case 4, the percentage error of h was about 3% to 5%, and the percentage error of η was about 4% to 10%. For case 5, the percentage error of h was below 2%, and the percentage error of η was below 1%.

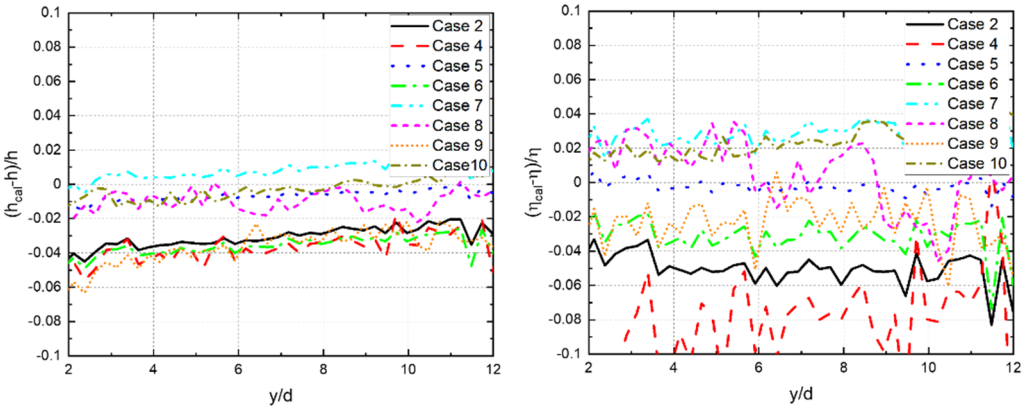

Figure 11. Errors of calculated span-wise averaged heat transfer coefficient and film cooling effectiveness at M = 1.0.

4. Discussion

In this paper, flat plate film cooling with two rows of compound angle cylindrical film cooling holes was investigated. The method to calculate the film cooling effectiveness and heat transfer coefficient simultaneously from the transient wall temperature data was evaluated. Results showed that the method could be applied with time-dependent mainstream temperature and coolant temperature, where the film cooling effectiveness and heat transfer coefficient were constants. Furthermore, reliable results could be obtained when the wall temperature data at several times were known.

In general, the calculated film cooling effectiveness and heat transfer coefficient obtained by the method agreed well with the known data. Errors of film cooling effectiveness and heat transfer coefficient decreased when the heat transfer coefficient increased, as the uncertainty of the inverse method decreased. As the calculation was based on the one-dimensional heat conduction equation, in the region with high lateral heat conduction, large errors in film cooling effectiveness and heat transfer coefficient were observed. Lower thermal conductivity material could be used to reduce the lateral heat conduction effect. When the material thermal conductivity was 0.05 W/(m·K), the local error of η was mainly below 0.04, and the local percentage error of h was mainly below 6%. In terms of span-wise averaged film cooling effectiveness and heat transfer coefficient, the calculation and data were in very good agreement. Results showed that the percentage error of span-wise averaged η was mainly between 0% and 10%, and the percentage error of the span-wise averaged h was mainly between 0% and 4%.

Funding: This research received no external funding.

Institutional Review Board Statement: Not applicable.

Informed Consent Statement: Not applicable.

Conflicts of Interest: The author declares no conflict of interest.

Nomenclature

Cp	specific heat capacity (J/kg·K)
DR	coolant to mainstream density ratio = ρ_c/ρ_m
d	film cooling hole diameter (m)
h	heat transfer coefficient (W/m^2·K)
k	thermal conductivity (W/m·K)
M	coolant to mainstream blowing ratio = $\rho_c V_c/\rho_m V_m$
q	heat flux (W/m^2)
T_{aw}	adiabatic wall temperature (K)
T_c	coolant temperature (K)
T_m	mainstream temperature (K)
T_w	wall temperature (K)
t	time (s)
x	span-wise direction
y	stream-wise direction
z	inward-pointing normal direction of the wall
Greek Symbols	
η	film cooling effectiveness
α	hole inclination angle to the surface (^{o})
β	hole compound angle to the mainstream (^{o})
ρ	density (kg/m^3)
Subscripts	
c	coolant
m	mainstream
w	wall

References

1. Bogard, D.G.; Thole, K.A. Gas Turbine Film Cooling. *AIAA J. Propul. Power* **2006**, *22*, 249–270. [CrossRef]
2. Han, J.C.; Rallabandi, A.P. Turbine Blade Film Cooling Using PSP Technique. *Front. Heat Mass Transf.* **2010**, *1*, 013001. [CrossRef]
3. Han, J.C. Fundamental Gas Turbine Heat Transfer. *J. Therm. Sci. Eng. Appl.* **2013**, *5*, 021007. [CrossRef]
4. Ekkad, S.V.; Han, J.C. A Review of Hole Geometry and Coolant Density Effect on Film Cooling. In Proceedings of the Heat Transfer Summer Conference, Minneapolis, MN, USA, 14–19 July 2015; Volume 55492, p. V003T20A003.
5. Vedula, R.P.; Metzger, D.E. A Method for the Simultaneous Determination of Local Effectiveness and Heat Transfer Distributions in Three-Temperature Convective Situations. In Proceedings of the International Gas Turbine and Aeroengine Congress and Exposition, Orlando, FL, USA, 3–6 June 1991.
6. Ekkad, S.V.; Ou, S.C.; Rivir, R.B. A Transient Infrared Thermography Method for Simultaneous Film Cooling Effectiveness and Heat Transfer Coefficient Measurements from a Single Test. *J. Turbomach.* **2004**, *126*, 597–603. [CrossRef]
7. Cook, W.J.; Felderman, E.J. Reduction of data from thin-film heat-transfer gages—A concise numerical technique. *AIAA J.* **1966**, *4*, 561–562. [CrossRef]
8. Walker, D.G.; Scott, E.P. Evaluation of Estimation Methods for High Unsteady Heat Fluxes from Surface Measurements. *J. Thermophys. Heat Transf.* **1998**, *12*, 543–551. [CrossRef]
9. Oldfield, M.L.G. Impulse Response Processing of Transient Heat Transfer Gauge Signals. *J. Turbomach.* **2008**, *130*, 021023. [CrossRef]
10. O'Dowd, D.O.; Zhang, Q.; He, L.; Ligrani, P.M.; Friedrichs, S. Comparison of Heat Transfer Measurement Techniques on a Transonic Turbine Blade Tip. *J. Turbomach.* **2011**, *133*, 021028. [CrossRef]
11. Peck, J.; Liu, J.; Bryden, K.M.; Shih, T.I.-P. Methods for Measuring and Computing the Adiabatic-Wall Temperature. In Proceedings of the International Gas Turbine and Aeroengine Congress and Exposition, Virtual Conference, 21–25 September 2020.
12. Schmidt, D.L.; Sen, B.; Bogard, D.G. Film Cooling with Compound Angle Holes: Adiabatic Effectiveness. *J. Turbomach.* **1996**, *118*, 807–813. [CrossRef]
13. Sen, B.; Schmidt, D.L.; Bogard, D.G. Film Cooling with Compound Angle Holes: Heat Transfer. *J. Turbomach.* **1996**, *118*, 800–806. [CrossRef]
14. Ekkad, S.V.; Zapata, D.; Han, J.C. Film Effectiveness Over a Flat Surface with Air and CO_2 Injection Through Compound Angle Holes Using a Transient Liquid Crystal Image Method. *J. Turbomach.* **1997**, *119*, 587–593. [CrossRef]
15. Ekkad, S.V.; Zapata, D.; Han, J.C. Heat Transfer Coefficients Over a Flat Surface with Air and CO_2 Injection Through Compound Angle Holes Using a Transient Liquid Crystal Image Method. *J. Turbomach.* **1997**, *119*, 580–586. [CrossRef]
16. Ekkad, S.V.; Han, J.C. A transient liquid crystal thermography technique for gas turbine heat transfer measurements. *Meas. Sci. Technol.* **2000**, *11*, 957–968. [CrossRef]

17. Chen, A.F.; Li, S.J.; Han, J.C. Film Cooling for Cylindrical and Fan-Shaped Holes Using Pressure-Sensitive Paint Measurement Technique. *J. Thermophys. Heat Transf.* **2015**, *29*, 1–10. [CrossRef]
18. Laroche, E.; Donjat, D.; Reulet, P. A Combined Experimental and Numerical Characterization of the Flowfield and Heat Transfer around a Multiperforated Plate with Compound Angle Injection. *Energies* **2021**, *14*, 613. [CrossRef]
19. Yao, J.X.; Xu, J.; Zhang, K.; Lei, J.; Wright, L.M. Interaction of Flow and Film-Cooling Effectiveness Between Double-Jet Film-Cooling Holes with Various Spanwise Distances. *J. Turbomach.* **2018**, *140*, 121011. [CrossRef]
20. Yao, J.X.; Zhang, K.; Wu, J.M.; Lei, J.; Fang, Y.; Wright, L.M. An experimental investigation on streamwise distance and density ratio effects on double-jet film-cooling. *Appl. Therm. Eng.* **2019**, *156*, 410–421. [CrossRef]
21. Yao, J.X.; Su, P.F.; He, J.H.; Wu, J.M.; Lei, J.; Fang, Y. Experimental and numerical investigations on double-jet film-cooling with different mainstream incidence angles. *Appl. Therm. Eng.* **2020**, *166*, 114737. [CrossRef]
22. Hang, J.; Zhang, J.Z.; Wang, C.H.; Shan, Y. Numerical Investigation of Single-Row Double-Jet Film Cooling of a Turbine Guide Vane under High-Temperature and High-Pressure Conditions. *Energies* **2022**, *15*, 287. [CrossRef]
23. Wang, N.; Zhang, M.J.; Shiau, C.C.; Han, J.C. Film Cooling Effectiveness from Two Rows of Compound Angled Cylindrical Holes Using Pressure-Sensitive Paint Technique. *J. Heat Transf.* **2019**, *141*, 042202. [CrossRef]
24. Zhang, M.J.; Si, W.F.; Lee, C.B. Heat Transfer and Recovery Factor of Aerodynamic Heating on a Flared Cone. *AIAA J.* **2021**, *59*, 4284–4292. [CrossRef]